

# Modelling and performance analysis of a curvature-adjustable multiple-axis flexure hinge based on Bézier curve

Proc IMechE Part C:  
J Mechanical Engineering Science  
1–14  
© IMechE 2023  
Article reuse guidelines:  
sagepub.com/journals-permissions  
DOI: 10.1177/09544062231206660  
journals.sagepub.com/home/pic  


Xuwen Wang<sup>1,2</sup> , Yang Yu<sup>1,3</sup>, Zhenbang Xu<sup>1,2,3</sup>,  
Anpeng Xu<sup>1,2</sup> and Chao Qin<sup>1,3</sup>

## Abstract

In order to solve the uniqueness of the compliance equations and each notch profile, a curvature-adjustable multiple-axis flexure hinge with complex notch profiles is designed and investigated based on Bézier curve in this paper. The hinge can evolve into multiple-axis flexure hinges with single and hybrid, symmetric and asymmetric notch profiles composed of the ellipse, circle, hyperbola and parabola. In addition, analytical compliance equations in six degrees of freedom based on the Castigliano's Second Theorem are proposed. Then, a simplified notch profile classification method based on a binary quadratic implicit equation is proposed. Moreover, analytical compliance equations are validated by finite element analysis. The maximum relative error between the finite element analysis and the analytical results is 6.07%. Finally, the compliance, precision of rotation and stress are investigated based on structural parameters. The results show that the change in the rotation centre does not significantly affect the axial and bending compliance for the flexure hinge with a specific single and flush Bézier curve notch profile. Moreover, the flexure hinge with a notch profile consisting of ellipse and hyperbola has the highest rotational precision. The proposed curvature-adjustable multiple-axis flexure hinge can provide more compliance options for the design of compliant mechanisms.

## Keywords

Flexure hinges, compliance equation, multiple-axis, Bézier curve, curvature-adjustable

Date received: 19 March 2023; accepted: 16 September 2023

## Introduction

With the rapid development of micro and nano processing technology and precision positioning technology, flexure hinges are widely used in large aperture telescopes,<sup>1</sup> vibration sensors,<sup>2</sup> micro-accelerometers<sup>3</sup> and parallel manipulators.<sup>4</sup>

Flexure hinges perform the function of rotation by generating elastic deformation, which avoids the friction and backlash of conventional hinges. It is worth noting that the compliance of flexure hinges depends mainly on the notch profile.<sup>5</sup> In order to meet the requirements of large range of motion, high axial stiffness and low stress concentration, flexure hinges with different notch profiles have been designed and developed one after another. For example, circular flexure hinge (CCFH),<sup>6,7</sup> elliptical flexure hinge (EPFH),<sup>8–11</sup> leaf spring flexure hinge (LSFH),<sup>12,13</sup> corner- filleted flexure hinge (CFFH),<sup>14,15</sup> parabolic flexure hinge (PAFH),<sup>16–18</sup> hyperbolic flexure hinge (HYFH),<sup>18</sup> cycloidal flexure hinge (CYFH),<sup>19,20</sup> filleted V-shaped flexure hinge (FVFH),<sup>19–21</sup> power-function-shaped flexure hinge (PFFH),<sup>22</sup> right-circular corner-filleted

flexure hinge (RCCF),<sup>23,24</sup> right-circular elliptical flexure hinge (RCEP),<sup>23,24</sup> exponent-sine-shaped flexure hinge (ESFH),<sup>25</sup> nonsymmetric elliptical circular flexure hinge (NSEC),<sup>26</sup> etc.

It is remarkable that these works are limited to flexure hinges with a single sensitive axis transverse notch profile. Moreover, it is too cumbersome to use

<sup>1</sup>Changchun Institute of Optics, Fine Mechanics and Physics, Chinese Academy of Sciences, Changchun, China

<sup>2</sup>University of Chinese Academy of Sciences, Beijing, China

<sup>3</sup>Chinese Academy of Science Key Laboratory of On-orbit Manufacturing and Integration for Space Optics System, Changchun, China

### Corresponding authors:

Yang Yu, Changchun Institute of Optics, Fine Mechanics and Physics, Chinese Academy of Sciences, No. 3888 Dong Nanhu Road, Changchun, Jilin 130033, China.  
Email: yuyang@ciomp.ac.cn

Zhenbang Xu, Changchun Institute of Optics, Fine Mechanics and Physics, Chinese Academy of Sciences, No. 3888 Dong Nanhu Road, Changchun, Jilin 130033, China.  
Email: xuzhenbang@ciomp.ac.cn

different compliance equations to design flexure hinges with different notch profiles. Therefore, generalised closed-form compliance equations for the parametric design of hinges would allow a more comprehensive consideration of the compliance of various notch profiles. The generalised compliance equations described here should be able to be applied to flexure hinges with a wide range of notch profiles.

Some investigations have been carried out intensively to solve this issue. Kong et al.<sup>27</sup> have investigated conic-V-shaped flexure hinges. Wu et al. have parameterised conical notched flexure hinges using non-uniform rational B-spline (NURBS) curve, which include elliptic, parabolic, and hyperbolic notch curves.<sup>28</sup> Li et al. have analysed and modelled hybrid flexure hinges.<sup>29</sup> However, these efforts have mainly focused on flexure hinges with a single sensitive axis transversely notched. In order to meet the demand for multi-degree-of-freedom movements in spatial compliant mechanisms, flexure hinges with two-sensitive-axis transverse notches and multi-sensitive-axis rotational notches have also been developed and investigated.<sup>30–32</sup> Li et al. have proposed a generalised two-axis elliptical-arc- filleted flexure hinge to satisfy the need for two-degree-of-freedom motion.<sup>30</sup> Then, for the requirement of multi-degree-of-freedom motion of the spatial compliant mechanism, Li et al. have proposed the generalised model and configuration design of multiple-axis flexure hinges.<sup>33</sup> However, the compliance model needs to rely on the existing compliance equations. Then, Wang et al. have presented the compliance equations for the generalised elliptic-arc beam spherical flexure hinge.<sup>34</sup> Wei et al. have derived the closed-form compliance equation for elliptic-revolve notch type multiple-axis flexure hinges.<sup>35</sup> Additionally, Wei et al. have analysed the compliance and experimental principles of hybrid multiple-axis flexure hinges.<sup>36</sup> Lastly, Ling et al. have proposed a generalised flexure hinge based on a discrete-beam transfer matrix.<sup>37</sup> However, most of the above investigations need to rely on different compliance equations. In addition, Ling et al. have already proposed curvature-adjustable flexure hinge inspired by red blood cells.<sup>38</sup> However, the notch profile types in this investigation are limited.

In order to avoid wasting a lot of time in finding different compliance equations to design flexure hinges, a curvature-adjustable flexure hinge needs to be proposed. The curvature-adjustable property can be used to design the hinges with common notch profiles.

The main contribution is the development of a curvature-adjustable multiple-axis flexure hinge based on the Bézier curve in this paper. The curvature-adjustable property can be applied to the design of multiple-axis hinges with common notch profiles, which are mainly composed of circles, ellipses, hyperbolas, and parabolas. Then, a simplified classification

method of notch profiles based on a binary quadratic implicit equation is proposed. In addition, analytical compliance equations are verified by finite element analysis. Then, the compliance, precision of rotation, and stress are investigated based on structural parameters. Finally, some conclusions are given.

## Compliance equations

A quadratic Bézier curve is a curve from three control points. The first control point defines the start of the curve, and the third control point defines its end. The intermediate control point influences the curvature of the curve, and it usually is not on the curve. To facilitate the establishment of the closed-form compliance equations for curvature-adjustable multiple-axis flexure hinges, the curve can be expressed as

$$\begin{bmatrix} x(t) \\ y(t) \end{bmatrix} = \frac{B_0^2(t)\mathbf{P}_0 + wB_1^2(t)\mathbf{P}_1 + B_2^2(t)\mathbf{P}_2}{B_0^2(t) + wB_1^2(t) + B_2^2(t)}, \quad (1)$$

where  $\mathbf{P}_0 = [x_0, y_0]$ ,  $\mathbf{P}_1 = [x_1, y_1]$ , and  $\mathbf{P}_2 = [x_2, y_2]$  are the three control points of the curve.  $w$  is the weight of the point  $\mathbf{P}_1$ . When  $w = 0$ , the curve is a straight line. When  $0 < w < 1$ , the curve is an ellipse. When  $w = 1$ , the curve is a parabola. When  $w > 1$ , the curve is a hyperbola. In addition,  $t \in [0, 1]$ .

$B_n^i(t)$  ( $i = 0, 1, \dots, n$ ) is the Bernstein polynomials with degree  $n$ , which can be expressed as

$$B_i^n(t) = \frac{n!}{i!(n-i)!} t^i (1-t)^{n-i}, \quad (2)$$

where  $n = 2$ .

Then, the curve can be expressed as

$$x(t) = \frac{(1-t)^2 x_0 + 2wt(1-t)x_1 + t^2 x_2}{(1-t)^2 + 2wt(1-t) + t^2}, \quad (3)$$

$$y(t) = \frac{(1-t)^2 y_0 + 2wt(1-t)y_1 + t^2 y_2}{(1-t)^2 + 2wt(1-t) + t^2}. \quad (4)$$

In order to enrich the notch profile types of multiple-axis flexure hinges as much as possible, the closed-form compliance equations can be established below. As shown in Figure 1, the notch profile of the flexure hinge consists of three parts, which are a Bézier curve, a straight line, and a Bézier curve. The lengths of the three parts are  $l_1$ ,  $l_2$  and  $l_3$ , respectively. And the total length is  $L = l_1 + l_2 + l_3$ .  $\mathbf{P}_0 = [x_0, y_0]$ ,  $\mathbf{P}_1 = [x_1, y_1]$ , and  $\mathbf{P}_2 = [x_2, y_2]$  are the three control points of the left Bézier curve  $m$ . And  $\mathbf{P}_3 = [x_3, y_3]$ ,  $\mathbf{P}_4 = [x_4, y_4]$ , and  $\mathbf{P}_5 = [x_5, y_5]$  are the three control points of the right Bézier curve  $n$ . The curve  $m$  and curve  $n$  can be expressed as

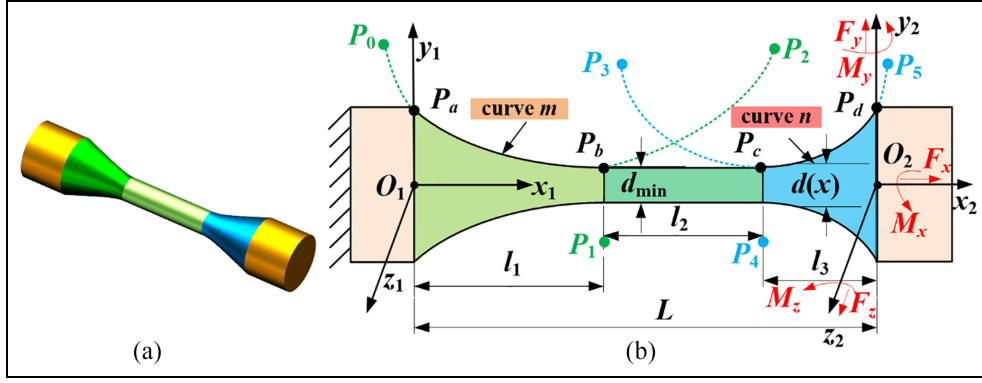


**Figure 1.** Multiple-axis flexure hinges: (a) 3D model and (b) geometric parameters.

$$\begin{bmatrix} x_m(t) \\ y_m(t) \end{bmatrix} = \frac{(1-t)^2 \mathbf{P}_0 + 2w_m t(1-t) \mathbf{P}_1 + t^2 \mathbf{P}_2}{(1-t)^2 + 2w_m t(1-t) + t^2}, \quad (5)$$

$$\begin{bmatrix} x_n(t) \\ y_n(t) \end{bmatrix} = \frac{(1-t)^2 \mathbf{P}_3 + 2w_n t(1-t) \mathbf{P}_4 + t^2 \mathbf{P}_5}{(1-t)^2 + 2w_n t(1-t) + t^2}, \quad (6)$$

where  $w_m$  is the weight of  $\mathbf{P}_1$  and  $w_n$  is the weight of  $\mathbf{P}_4$ .

In addition,  $\mathbf{P}_a$  and  $\mathbf{P}_b$  are the boundary points of the left curve  $m$ . Then,  $\mathbf{P}_c$  and  $\mathbf{P}_d$  are the boundary points of the right curve  $n$ . These points can be expressed as

$$\begin{aligned} \mathbf{P}_a &= \begin{bmatrix} x_m(t_1) \\ y_m(t_1) \end{bmatrix}, \mathbf{P}_b = \begin{bmatrix} x_m(t_2) \\ y_m(t_2) \end{bmatrix}, \\ \mathbf{P}_c &= \begin{bmatrix} x_n(t_3) \\ y_n(t_3) \end{bmatrix}, \mathbf{P}_d = \begin{bmatrix} x_n(t_4) \\ y_n(t_4) \end{bmatrix}. \end{aligned} \quad (7)$$

As shown in Figures 1(b) and 2(a), it should be noted that the Bézier curve formed by unconstrained control points is difficult to determine the minimum diameter  $d_{min}$ . It is because the location of the lowest point is difficult to be determined. However, taking the curve  $m$  as an example, the control points of the curve can be expressed as

$$\mathbf{P}_{01} = \frac{\mathbf{P}_0 + w\mathbf{P}_1}{1+w}, \quad (8)$$

$$\mathbf{P}_{21} = \frac{\mathbf{P}_2 + w\mathbf{P}_1}{1+w}, \quad (9)$$

$$\mathbf{P}_m = \frac{\mathbf{P}_2 + \mathbf{P}_0}{2}, \quad (10)$$

$$\mathbf{P}_b = \frac{\mathbf{P}_m + w\mathbf{P}_1}{1+w} = \frac{\mathbf{P}_0 + 2w\mathbf{P}_1 + \mathbf{P}_2}{2(1+w)}. \quad (11)$$

Therefore, to facilitate the design of the flexure hinge, set  $y_0 = y_2$ , as shown in Figure 2(b). Similarly set  $y_3 = y_5$ . At this time, the minimum diameter  $d_{min}$  can be expressed as

$$d_{min} = 2y_m(t_2) = 2y_n(t_3). \quad (12)$$

Thus, the diameter  $d(x)$  of the hinge can be expressed as

$$d(x) = \begin{cases} 2y_m(t) & t \in [t_1, t_2] \\ d_{min} & x \in [l_1, l_1 + l_2] \\ 2y_n(t) & t \in [t_3, t_4] \end{cases} \quad (13)$$

Then, the cross-sectional area  $A(x)$  can be expressed as

$$A(x) = \begin{cases} \pi y_m^2(t) & t \in [t_1, t_2] \\ \frac{\pi d_{min}^2}{4} & x \in [l_1, l_1 + l_2] \\ \pi y_n^2(t) & t \in [t_3, t_4] \end{cases} \quad (14)$$

In addition, the moment of inertia about the cross-sectional area of the neutral axis can be expressed as

$$I_y(x) = I_z(x) = \begin{cases} \frac{\pi y_m^4(t)}{4} & t \in [t_1, t_2] \\ \frac{\pi d_{min}^4}{64} & x \in [l_1, l_1 + l_2] \\ \frac{\pi y_n^4(t)}{4} & t \in [t_3, t_4] \end{cases} \quad (15)$$

In this moment, the hybrid multiple-axis flexure hinge can be considered as a variable-section cantilever beam with one side fixed. The coordinate system is defined at the fixed end, as shown in Figure 1(b). When the external load vector  $\mathbf{F} = [F_x, F_y, F_z, M_x, M_y, M_z]^T$  acts on the node  $O_2$  at the free end of the flexure hinge, the flexure hinge is deformed. The displacement vector is  $\mathbf{\Delta} = [\Delta_x, \Delta_y, \Delta_z, \theta_x, \theta_y, \theta_z]^T$ . In

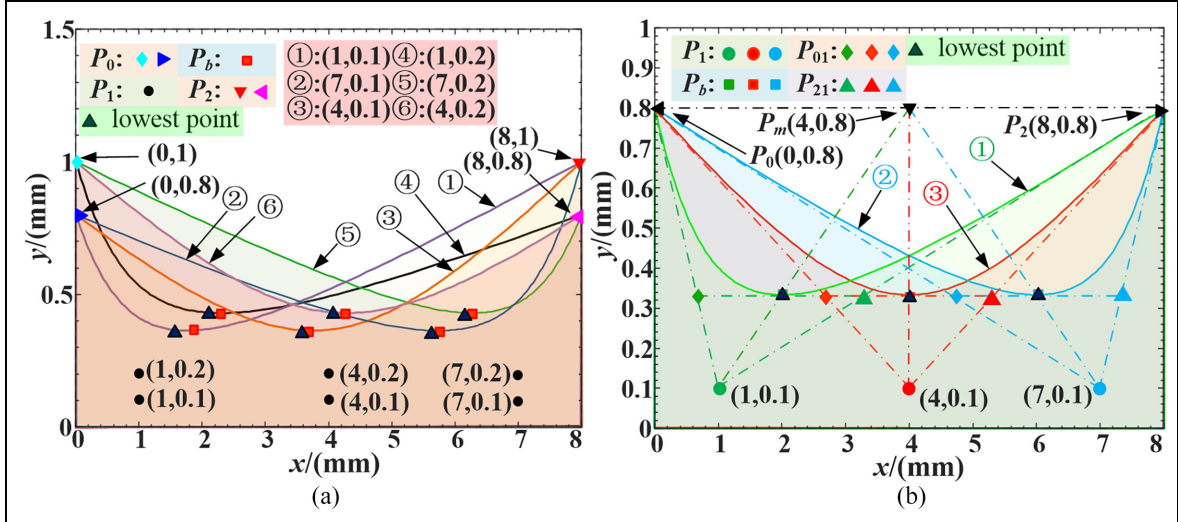


**Figure 2.** Parameterised Bézier curves ( $w = 2$ ): (a)  $y_0 \neq y_2$  and (b)  $y_0 = y_2$ .

addition, the total elastic strain energy of the hybrid multiple-axis flexure hinge includes strain energy from tension or compression, shear, bending, and torsion. Therefore, the total strain energy can be expressed as

$$U = \int_0^L \frac{F_x^2(x)}{2EA(x)} dx + \int_0^L \frac{\kappa F_y^2(x)}{2GA(x)} dx + \int_0^L \frac{\kappa F_z^2(x)}{2GA(x)} dx + \int_0^L \frac{M_x^2(x)}{2GI_p(x)} dx + \int_0^L \frac{M_y^2(x)}{2EI_y(x)} dx + \int_0^L \frac{M_z^2(x)}{2EI_z(x)} dx \quad (16)$$

where  $E$  is the elastic modulus,  $G$  is the shear modulus, and the shear coefficient  $\kappa$  is  $10/9$ .  $I_p(x)$  is the polar moment of inertia of the cross section.

Then, the external load vector  $\mathbf{F}$  can be expressed as

$$\begin{cases} F_x(x) = F_x, M_x(x) = M_x \\ F_y(x) = F_y, M_y(x) = M_y - F_z(L - x) \\ F_z(x) = F_z, M_z(x) = M_z + F_y(L - x) \end{cases} \quad (17)$$

Therefore, the relationship between the load  $\mathbf{F}$  and the deformation  $\Delta$  can be expressed as

$$\Delta = \mathbf{CF}, \quad (18)$$

in which

$$\mathbf{C} = \begin{bmatrix} C_{\Delta_x-F_x} & 0 & 0 & 0 & 0 & 0 \\ 0 & C_{\Delta_y-F_y} & 0 & 0 & 0 & C_{\Delta_y-M_z} \\ 0 & 0 & C_{\Delta_z-F_z} & 0 & C_{\Delta_z-M_y} & 0 \\ 0 & 0 & 0 & C_{\theta_x-M_x} & 0 & 0 \\ 0 & 0 & C_{\theta_y-F_z} & 0 & C_{\theta_y-M_y} & 0 \\ 0 & C_{\theta_z-F_y} & 0 & 0 & 0 & C_{\theta_z-M_z} \end{bmatrix} \quad (19)$$

Based on Castigliano's Second Theorem, the partial derivative of the strain energy  $U$  to the external load  $\mathbf{F}$  equals the displacement  $\Delta$  of the loading point, which can be descriptively expressed as

$$\Delta = \frac{\partial U}{\partial \mathbf{F}}. \quad (20)$$

Then, the compliance matrix  $\mathbf{C}$  is analysed in combination with equations (16)–(20).

Initially, the axial compliance  $C_{\Delta_x-F_x}$  can be expressed as

$$\begin{aligned} C_{\Delta_x-F_x} &= \int_0^L \frac{dx}{EA(x)} \\ &= \frac{1}{\pi E} \left( \int_{t_1}^{t_2} \frac{x'_m(t)}{y_m^2(t)} dt + \int_{t_3}^{t_4} \frac{x'_n(t)}{y_n^2(t)} dt + \int_{t_1}^{t_1+t_2} \frac{1}{y_m^2(t_2)} dx \right) \\ &= \frac{1}{\pi E} \left( N_1 + N_2 + \int_{t_1}^{t_1+t_2} \frac{1}{y_m^2(t_2)} dx \right) \end{aligned} \quad (21)$$

where  $N_1$  and  $N_2$  can be expressed as

$$N_1 = \int_{t_1}^{t_2} \frac{x'_m(t)}{y_m^2(t)} dt, N_2 = \int_{t_3}^{t_4} \frac{x'_n(t)}{y_n^2(t)} dt. \quad (22)$$

Then,  $C_{\Delta_y-F_y}$  and  $C_{\Delta_z-F_z}$  can be expressed as

$$C_{\Delta_y-F_y} = C_{\Delta_z-F_z} = C_{\Delta_y^s-F_y} + C_{\Delta_y^b-F_y}, \quad (23)$$

in which

$$C_{\Delta_y^s-F_y} = \frac{\kappa}{\pi G} \left( N_1 + N_2 + \frac{l_2}{y_m^2(t_2)} \right), \quad (24)$$

$$\begin{aligned}
C_{\Delta_y-F_y} &= \frac{1}{E} \int_0^L \frac{(L-x)^2 dx}{I_y(x)} \\
&= \frac{4L^2}{\pi E} (N_3 + N_6) - \frac{8L}{\pi E} (N_4 + N_7) + \\
&\quad \frac{4}{\pi E} (N_5 + N_8) + \frac{4((L-l_1)^3 - (L-l_2-l_1)^3)}{3\pi E y_m^4(t_2)}
\end{aligned} \quad (25)$$

where  $N_i$  ( $i = 3, \dots, 8$ ) can be expressed as

$$\begin{cases}
N_3 = \int_{t_1}^{t_2} \frac{x'_m(t)}{y_m^4(t)} dt, N_4 = \int_{t_1}^{t_2} \frac{x_m(t)x'_m(t)}{y_m^4(t)} dt \\
N_5 = \int_{t_1}^{t_2} \frac{x_m^2(t)x'_m(t)}{y_m^4(t)} dt, N_6 = \int_{t_3}^{t_4} \frac{x'_n(t)}{y_n^4(t)} dt \\
N_7 = \int_{t_3}^{t_4} \frac{x_n(t)x'_n(t)}{y_n^4(t)} dt, N_8 = \int_{t_3}^{t_4} \frac{x_n^2(t)x'_n(t)}{y_n^4(t)} dt
\end{cases} \quad (26)$$

In addition, the rotational compliances can be expressed as

$$\begin{aligned}
C_{\Delta_y-M_z} &= C_{\theta_z-F_y} = -C_{\Delta_z-M_y} = -C_{\theta_y-F_z} \\
&= \frac{1}{E} \int_0^L \frac{L-x}{I_y(x)} dx = \frac{4L(N_3 + N_6)}{\pi E} + \frac{4Ll_2}{\pi E y_m^4(t_2)} \\
&\quad - \frac{4(N_4 + N_7)}{\pi E} - \frac{2((l_2 + l_1)^2 - l_1^2)}{\pi E y_m^4(t_2)}
\end{aligned} \quad (27)$$

$$\begin{aligned}
C_{\theta_z-M_z} &= C_{\theta_y-M_y} \\
&= \int_0^L \frac{1}{EI_y(x)} dx = \frac{4(N_3 + N_6)}{\pi E} + \frac{4l_2}{\pi E y_m^4(t_2)}
\end{aligned} \quad (28)$$

Finally, the torsional compliance  $C_{\theta_x-M_x}$  can be expressed as

$$C_{\theta_x-M_x} = \int_0^L \frac{1}{GI_p(x)} dx = \frac{2(N_3 + N_6)}{G\pi} + \frac{2l_2}{G\pi y_m^4(t_2)}, \quad (29)$$

where  $I_p(x) = I_y(x) + I_z(x)$  is the polar moment of inertia of the cross section.

Compared with generalised compliance equations based on an elliptic curve, the generalised compliance equation based on the Bézier curve contains more types of notches.

## Notch profiles of the flexure hinge

There is also a great difference in the performance of flexure hinges with different notch profiles. In order

to classify the notch profiles of multiple-axis flexure hinges, the analysis is based on a binary quadratic implicit equation. The binary quadratic implicit equation can be expressed as

$$ax^2 + bxy + cy^2 + dx + ey + f = 0, \quad (30)$$

in which<sup>39</sup>

$$\begin{aligned}
a &= y_0^2 - 4w^2 y_0 y_1 + 4w^2 y_1^2 - 2y_0 y_2 + 4w^2 y_0 y_2 \\
&\quad - 4w^2 y_1 y_2 + y_2^2
\end{aligned} \quad (31)$$

$$\begin{aligned}
b &= -2x_0 y_0 + 4w^2 x_1 y_0 - 4w^2 x_2 y_0 + 4w^2 x_0 y_1 \\
&\quad - 8w^2 x_1 y_1 + 4w^2 x_2 y_1 + 2x_0 y_2 - 4w^2 x_0 y_2 \\
&\quad + 4w^2 x_1 y_2 - 2x_2 y_2 + 2x_2 y_0
\end{aligned} \quad (32)$$

$$\begin{aligned}
c &= x_0^2 - 4w^2 x_0 x_1 + 4w^2 x_1^2 - 2x_0 x_2 + 4w^2 x_0 x_2 \\
&\quad - 4w^2 x_1 x_2 + x_2^2
\end{aligned} \quad (33)$$

$$\begin{aligned}
d &= -2x_2 y_0^2 + 4w^2 x_1 y_0 y_1 + 4w^2 x_2 y_0 y_1 - 4w^2 x_0 y_1^2 \\
&\quad - 4w^2 x_2 y_1^2 + 2x_0 y_0 y_2 - 8w^2 x_1 y_0 y_2 + 2x_2 y_0 y_2 \\
&\quad + 4w^2 x_0 y_1 y_2 + 4w^2 x_1 y_1 y_2 - 2x_0 y_2^2
\end{aligned} \quad (34)$$

$$\begin{aligned}
e &= -4w^2 x_1^2 y_0 + 2x_0 x_2 y_0 + 4w^2 x_1 x_2 y_0 - 2x_2^2 y_0 \\
&\quad + 4w^2 x_0 x_1 y_1 - 8w^2 x_0 x_2 y_1 + 4w^2 x_1 x_2 y_1 - 2x_0^2 y_2 \\
&\quad + 4w^2 x_0 x_1 y_2 - 4w^2 x_1^2 y_2 + 2x_0 x_2 y_2
\end{aligned} \quad (35)$$

$$\begin{aligned}
f &= x_2^2 y_0^2 - 4w^2 x_1 x_2 y_0 y_1 + 4w^2 x_0 x_2 y_1^2 + 4w^2 x_1^2 y_0 y_2 \\
&\quad - 2x_0 x_2 y_0 y_2 - 4w^2 x_0 x_1 y_1 y_2 + x_0^2 y_2^2
\end{aligned} \quad (36)$$

Take the curve  $m$  as an example, as shown in Figure 2(b). To facilitate the classification of the notch profiles, the conditions can be expressed as

$$x_1 = \frac{x_0 + x_2}{2}, y_0 = y_2. \quad (37)$$

At this point, equations (31)–(36) can be expressed as

$$a = 4w^2 (y_0 - y_1)^2 \quad (38)$$

$$b = 0 \quad (39)$$

$$c = (1 - w^2)(x_0 - x_2)^2 \quad (40)$$

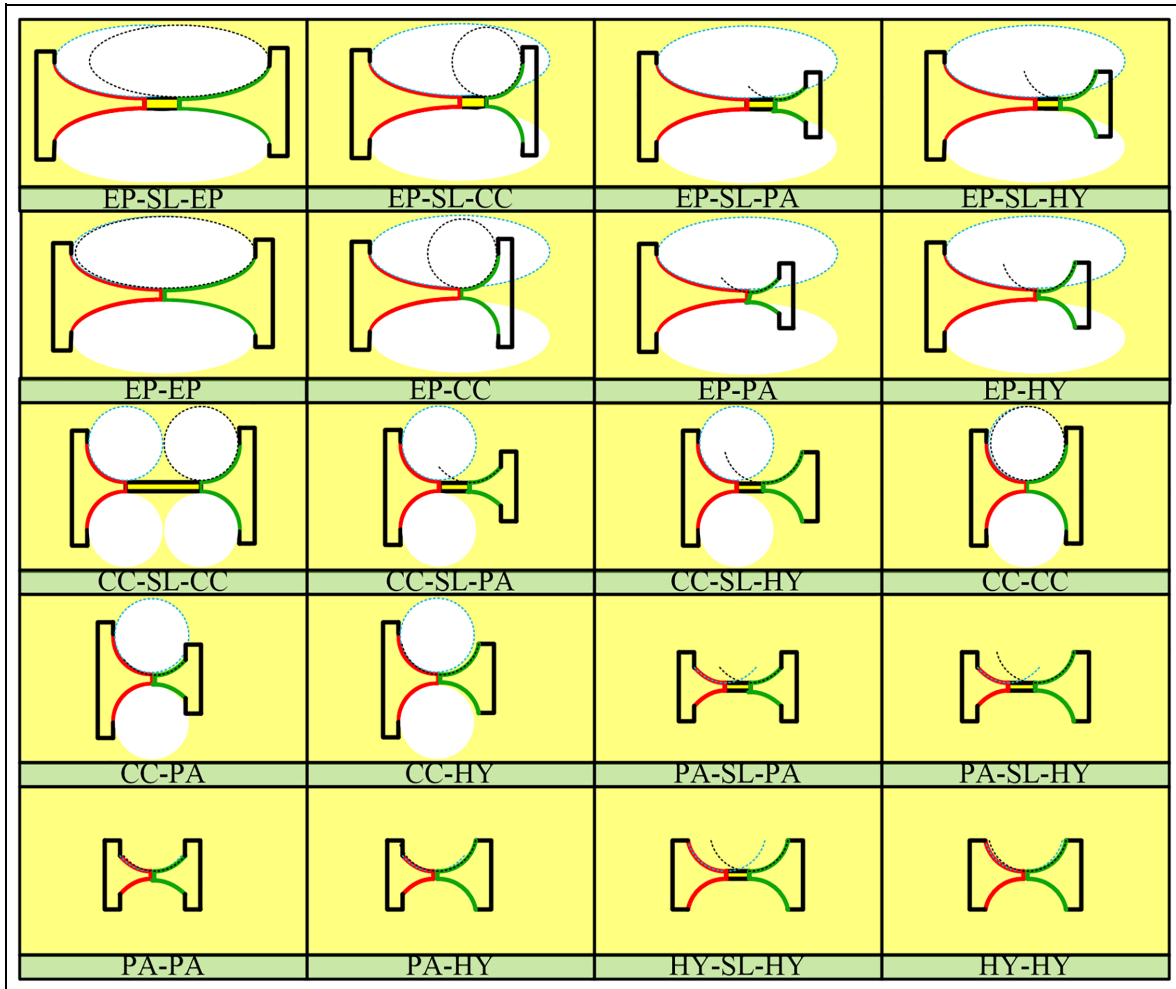


**Figure 3.** Notch profiles derived from multiple-axis flexure hinges ('-' simply indicates the type of notch in each section). Additionally, EP, PA, CC, HY and SL are abbreviations for ellipse, parabola, circle, hyperbola and straight line, respectively.

$$d = 16w^2x_1y_0y_1 - 8w^2x_1(y_1^2 + y_0^2) \quad (41)$$

$$e = 8w^2y_1(x_1^2 - x_0x_2) - 2y_2(x_0 - x_2)^2 \quad (42)$$

$$f = (x_0 - x_2)^2y_2^2 + 4w^2(x_1^2y_2^2 + x_0x_2y_1^2 - 2x_1^2y_1y_2). \quad (43)$$

When the curve is hyperbolic ( $c < 0$ ,  $w > 1$ ), equation (30) can be expressed as

$$\frac{(y + \frac{e}{2c})^2}{a} - \frac{(x + \frac{d}{2a})^2}{(-c)} = \frac{1}{ac}(\frac{d^2}{4a} + \frac{e^2}{4c} - f). \quad (44)$$

When the curve is parabolic ( $w = 1$ ), equation (30) can be expressed as

$$ax^2 + dx + ey + f = 0. \quad (45)$$

When the curve is elliptical ( $0 < w < 1$ ), equation (30) can be expressed as

$$\frac{(x + \frac{d}{2a})^2}{c} + \frac{(y + \frac{e}{2c})^2}{a} = \frac{1}{ac}(\frac{d^2}{4a} + \frac{e^2}{4c} - f). \quad (46)$$

Specially, when  $a = c$ , the curve is a circle. Then, the weight  $w$  of  $P_1$  can be expressed as

$$w = \sqrt{\frac{(x_0 - x_2)^2}{(x_0 - x_2)^2 + 4(y_0 - y_1)^2}}. \quad (47)$$

Similarly, a similar operation is performed for the curve  $n$ . There are 20 types of derived notch profiles for flexure hinges based on Bézier curves, as shown in Figure 3. The most important thing is that there is a distinction between single and hybrid, and symmetrical and asymmetrical curves of the notches, so there are more types of hinges. Therefore, the multiple-axis flexure hinge provides more compliance options for the design and optimisation of spatial compliant mechanisms. In addition, the classification method makes it possible to represent the notch profile in a

**Table 1.** Geometric parameters of multiple-axis flexure hinges (unit: mm).

Hinge no.	$P_0, P_1, P_2$	$w_m$	$P_3, P_4, P_5$	$w_n$	$l_2$	Type
1	(0,2), (2,0), (4,2)	1	(2,2.5), (5, -0.5), (8,2.5)	1	3	PA-SL-PA
2	(0,2), (2,0), (4,2)	1	(2,2), (5, -1), (8,2)	0.5	3	PA-SL-EP
3	(0,2), (2,0), (4,2)	1	(2,3), (5,0), (8,3)	2	3	PA-SL-HY
4	(0,0.5), (2, -0.1), (4,0.5)	1	(0, 0.3), (2,0.1), (4, 0.3)	1	0	PA-PA
5	(0,0.5), (2, -0.1), (4,0.5)	1	(0,0.3), (2,0), (4,0.3)	0.5	0	PA-EP
6	(0,0.5), (2, -0.1), (4,0.5)	1	(0,0.6), (2,0), (4,0.6)	2	0	PA-HY
7	(0,1.5), (2,0), (4,1.5)	0.5	(2,2), (5, -1), (8,2)	0.5	3	EP-SL-EP
8	(0,1.5), (2,0), (4,1.5)	0.5	(2,3), (5,0), (8,3)	2	3	EP-SL-HY
9	(0,0.3), (2,0), (4,0.3)	0.5	(0,0.4), (2, -0.2), (4,0.4)	0.5	0	EP-EP
10	(0,0.3), (2,0), (4,0.3)	0.5	(0,0.8), (2,0), (4,0.8)	3	0	EP-HY
11	(0,1.5), (2,0), (4,1.5)	2	(2,3), (5,0), (8,3)	5	3	HY-SL-HY
12	(0,1.5), (2,0), (4,1.5)	4	(-2,1.5), (2,0), (6,1.5)	4	0	HY-HY

**Table 2.** Compliance results of the flexure hinge obtained by analytical equations and finite element analysis.

Hinge no.	$C_{\Delta x-Fx}$ (mm/N)	$C_{\Delta y-Fy}$ (mm/N)	$C_{\theta_x-M_x}$ (rad/N·mm)	$C_{\theta_z-F_y}$ (rad/N)	$C_{\theta_z-M_z}$ (rad/N·mm)
1 (Analytical)	$9.50 \times 10^{-6}$	$7.34 \times 10^{-4}$	$4.25 \times 10^{-5}$	$1.43 \times 10^{-4}$	$3.27 \times 10^{-5}$
1 (FEA)	$9.83 \times 10^{-6}$	$7.73 \times 10^{-4}$	$4.42 \times 10^{-5}$	$1.50 \times 10^{-4}$	$3.44 \times 10^{-5}$
2 (Analytical)	$1.01 \times 10^{-5}$	$7.41 \times 10^{-4}$	$4.55 \times 10^{-5}$	$1.46 \times 10^{-4}$	$3.50 \times 10^{-5}$
2 (FEA)	$1.03 \times 10^{-5}$	$7.79 \times 10^{-4}$	$4.69 \times 10^{-5}$	$1.52 \times 10^{-4}$	$3.68 \times 10^{-5}$
3 (Analytical)	$9.02 \times 10^{-6}$	$7.26 \times 10^{-4}$	$4.01 \times 10^{-5}$	$1.39 \times 10^{-4}$	$3.09 \times 10^{-5}$
3 (FEA)	$9.43 \times 10^{-6}$	$7.68 \times 10^{-4}$	$4.18 \times 10^{-5}$	$1.47 \times 10^{-4}$	$3.26 \times 10^{-5}$
4 (Analytical)	$1.06 \times 10^{-4}$	$2.99 \times 10^{-2}$	$1.05 \times 10^{-2}$	$1.41 \times 10^{-2}$	$8.10 \times 10^{-3}$
4 (FEA)	$1.07 \times 10^{-4}$	$3.02 \times 10^{-2}$	$1.06 \times 10^{-2}$	$1.42 \times 10^{-2}$	$8.14 \times 10^{-3}$
5 (Analytical)	$1.08 \times 10^{-4}$	$3.02 \times 10^{-2}$	$1.09 \times 10^{-2}$	$1.44 \times 10^{-2}$	$8.39 \times 10^{-3}$
5 (FEA)	$1.09 \times 10^{-4}$	$3.05 \times 10^{-2}$	$1.10 \times 10^{-2}$	$1.45 \times 10^{-2}$	$8.44 \times 10^{-3}$
6 (Analytical)	$8.13 \times 10^{-5}$	$2.70 \times 10^{-2}$	$7.18 \times 10^{-3}$	$1.17 \times 10^{-2}$	$5.52 \times 10^{-3}$
6 (FEA)	$8.20 \times 10^{-5}$	$2.73 \times 10^{-2}$	$7.25 \times 10^{-3}$	$1.18 \times 10^{-2}$	$5.59 \times 10^{-3}$
7 (Analytical)	$1.05 \times 10^{-5}$	$8.64 \times 10^{-4}$	$4.86 \times 10^{-5}$	$1.63 \times 10^{-4}$	$3.73 \times 10^{-5}$
7 (FEA)	$1.08 \times 10^{-5}$	$9.01 \times 10^{-4}$	$4.99 \times 10^{-5}$	$1.69 \times 10^{-4}$	$3.87 \times 10^{-5}$
8 (Analytical)	$9.50 \times 10^{-6}$	$8.49 \times 10^{-4}$	$4.32 \times 10^{-5}$	$1.56 \times 10^{-4}$	$3.32 \times 10^{-5}$
8 (FEA)	$9.88 \times 10^{-6}$	$8.89 \times 10^{-4}$	$4.48 \times 10^{-5}$	$1.63 \times 10^{-4}$	$3.48 \times 10^{-5}$
9 (Analytical)	$1.17 \times 10^{-4}$	$5.06 \times 10^{-2}$	$1.22 \times 10^{-2}$	$2.01 \times 10^{-2}$	$9.35 \times 10^{-3}$
9 (FEA)	$1.18 \times 10^{-4}$	$5.11 \times 10^{-2}$	$1.22 \times 10^{-2}$	$2.03 \times 10^{-2}$	$9.42 \times 10^{-3}$
10 (Analytical)	$9.16 \times 10^{-5}$	$4.71 \times 10^{-2}$	$9.06 \times 10^{-3}$	$1.74 \times 10^{-2}$	$6.97 \times 10^{-3}$
10 (FEA)	$9.37 \times 10^{-5}$	$4.77 \times 10^{-2}$	$9.16 \times 10^{-3}$	$1.77 \times 10^{-2}$	$7.06 \times 10^{-3}$
11 (Analytical)	$2.97 \times 10^{-5}$	$9.34 \times 10^{-3}$	$5.32 \times 10^{-4}$	$1.88 \times 10^{-3}$	$4.09 \times 10^{-4}$
11 (FEA)	$3.13 \times 10^{-5}$	$9.63 \times 10^{-3}$	$5.45 \times 10^{-4}$	$1.94 \times 10^{-3}$	$4.23 \times 10^{-4}$
12 (Analytical)	$3.09 \times 10^{-5}$	$1.16 \times 10^{-2}$	$1.04 \times 10^{-3}$	$3.01 \times 10^{-3}$	$8.03 \times 10^{-4}$
12 (FEA)	$3.28 \times 10^{-5}$	$1.22 \times 10^{-2}$	$1.08 \times 10^{-3}$	$3.17 \times 10^{-3}$	$8.44 \times 10^{-4}$

polar coordinate system, which provides a theoretical basis for the design and manufacture of hinges.

### Finite element analysis

In order to validate the closed-form compliance equation used to design the notch profile, 12 typical hinge examples are investigated by finite element analysis. Since the circle is a special case of ellipse, it is ignored. To facilitate the design of the hinge, it is necessary to state that  $t_1 = 0$ ,  $t_2 = t_3 = 0.5$  and  $t_4 = 1$ . The specific parameters are shown in Table 1.

The material of the flexure hinge is structural steel. elastic modulus is 200 GPa, Poisson's ratio is 0.3, and shear modulus is 76.92 GPa. The flexure hinge is meshed using PATRAN as shown in Figure 4. The element type of the grid is Tet 10. And its quality

should be higher than 80%. Additionally, the solution type is linear static. A fixed support is applied to the left end of the flexure hinge.  $F_y$  is applied to the left surface of the free end of the flexure hinge to eliminate parasitic moments. All other loads are applied to the right surface of the free end. The displacement of the flexure hinge is then evaluated mainly through points  $O_1$  and  $O_2$ . In addition, the rotation of the right surface is used to evaluate the angular deflection of the flexure hinge. The compliance results of the flexure hinges obtained from the analytical equations and finite element analysis are shown in Table 2. As shown in Figure 5, the maximum relative error between the finite element analysis and the analytical results is 6.07%. The simulation results prove the correctness of the closed-form compliance equation.

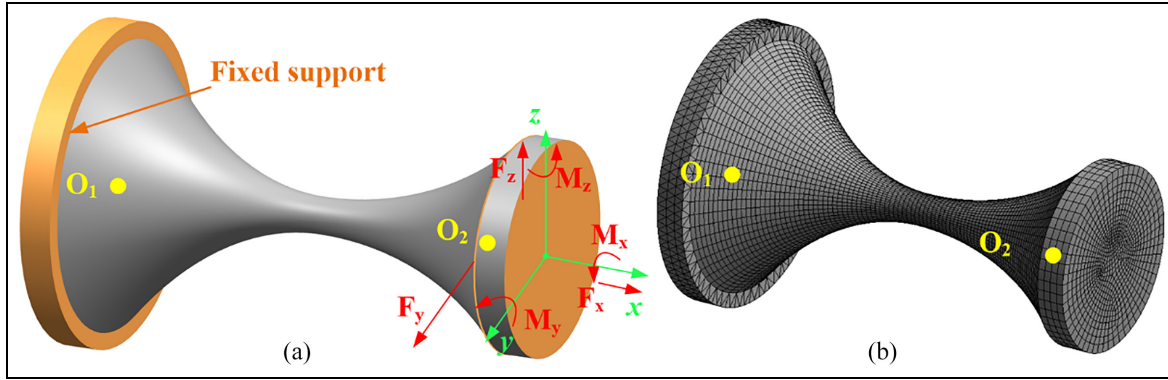


Figure 4. Multiple-axis flexure hinges: (a) the constraint and load settings and (b) the finite element model.

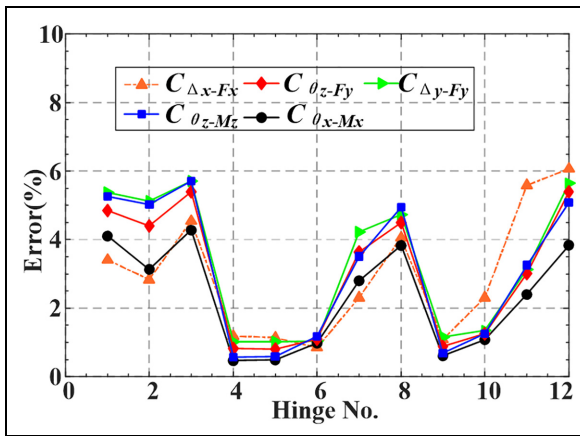


Figure 5. The relative error between the finite element analysis and the analytical results.

## Characteristics of flexure hinges

### Analysis of compliance characteristics

There are many parameters that affect the performance of the flexure hinge, mainly including control points ( $P_0, P_1, P_2, P_3, P_4$  and  $P_5$ ), the weights  $w$  ( $w_m, w_n$ ),  $l_2$ ,  $t$  ( $t_1, t_2, t_3, t_4$ ), etc. However, the large number of parameters does not facilitate the analysis of the effect of each parameter on the performance of the hinge. Therefore, it is a good choice to set the flexure hinge as a symmetrical flexure hinge. In other words, the left curve  $m$  is the same as the right curve  $n$ . Some necessary conditions can be expressed as

$$\begin{cases} w = w_m = w_n, y_0 = y_2 = y_3 = y_5 \\ x_1 = (x_0 + x_2)/2, x_3 = x_0 + l_2 \\ x_4 = x_1 + l_2, x_5 = x_2 + l_2 \end{cases} \quad (48)$$

Then, the effects of control points ( $P_1, P_4$ ), the weight  $w$  ( $w_m, w_n$ ), and  $l_2$  on the performance of the hinge are mainly investigated. At this point, the effect of  $w$  and  $l_2$  on the performance is shown in Figure 6. As  $w$  and  $l_2$  increase, the compliance of the hinge in each direction increases. Then, the control points

( $P_1, P_4$ ) not only affect the compliance, but also determine the rotation centre of the hinge. In other words, the control points can adjust the workspace of the hinge. In addition, the rotation centre is also related to  $l_2$ . In order to eliminate the effect of  $l_2$  and  $P_4$ , a flexure hinge with a single curve notch profile is investigated below. The constraint conditions can be expressed as

$$l_2 = l_3 = 0, t_1 = 0, t_2 = 1, t_3 = t_4 = 0. \quad (49)$$

Then, compliance equations can be expressed as

$$C_{\Delta x-Fx} = \frac{N_1}{\pi E} \quad (50)$$

$$C_{\Delta y-Fy} = C_{\Delta z-Fz} = \frac{\kappa N_1}{\pi G} + \frac{4L^2}{\pi E} N_3 - \frac{8L}{\pi E} N_4 + \frac{4}{\pi E} N_5 \quad (51)$$

$$\begin{aligned} C_{\Delta y-Mz} = C_{\theta_z-Fy} &= -C_{\Delta z-My} = -C_{\theta_y-Fz} \\ &= \frac{4LN_3}{\pi E} - \frac{4N_4}{\pi E} \end{aligned} \quad (52)$$

$$C_{\theta_z-Mz} = C_{\theta_y-My} = \frac{4N_3}{\pi E} \quad (53)$$

$$C_{\theta_x-Mx} = \frac{2N_3}{\pi G}. \quad (54)$$

In this case, the compliance and the rotation centre  $O$  of the hinge are only related to  $P_1$  and are not influenced by  $P_4$ , as shown in Figure 7. It is important to note that the effect of  $P_1$  on the compliance is only concentrated on  $N_1, N_3, N_4$  and  $N_5$ . Therefore, the related analysis can be equated to the analysis of the compliance in each direction. In addition, the rotation centre  $O$  of the hinge is only related to  $x_1$ . Therefore, it is necessary to focus on the effect of  $x_1$  on the compliance and the rotation centre. To investigate quantitatively the effect of  $x_1$  on the compliance,  $x_0 = 0$  and  $x_2 = 4$  (unit: mm) are set. As shown in Figure 8, when



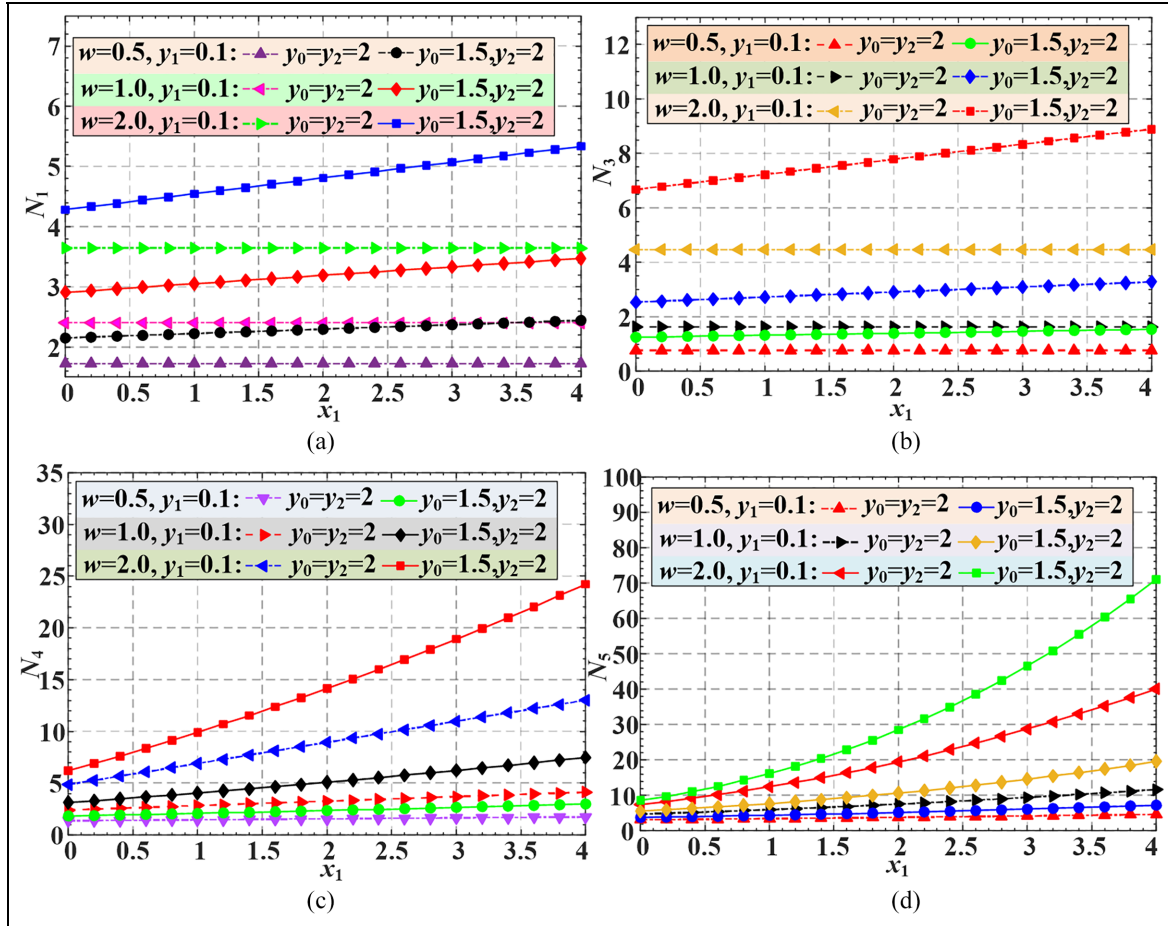


**Figure 8.** Influence of  $x_1$  on the compliance parameters: (a) influence of  $x_1$  on  $N_1$ , (b) influence of  $x_1$  on  $N_3$ , (c) influence of  $x_1$  on  $N_4$ , and (d) influence of  $x_1$  on  $N_5$ .

of  $x_1$ . In other words, when  $y_0 = y_2$  (the notch profile is flush), the compliance equations containing only  $N_1$  and  $N_3$  is little affected by  $x_1$ . In addition, the composition of the parameters in the compliance equation is very simple. Therefore, the analysis related to the effect of these parameters ( $N_1$ ,  $N_3$ ,  $N_4$  and  $N_5$ ) on the characteristic of the hinge is neglected.

The results show that when  $y_0 = y_2$ ,  $C_{\Delta x-Fx}$ ,  $C_{\theta z-Mz}$ ,  $C_{\theta y-My}$  and  $C_{\theta x-Mx}$  do not change significantly with the change of  $x_1$ . This means that a change in the rotation centre does not significantly change the compliance in some specific directions. Therefore, the performance of the compliant mechanism can be quickly improved by changing the rotation centre while satisfying the compliance in certain directions. It is useful to design the compliant mechanism.

### Precision of rotation

Currently, the parasitic motions of the geometry centre and the instant rotation centre are often used to evaluate the rotational precision of flexure hinges. Since part of the notch profile is asymmetric, the instant rotation centre of the hybrid multiple-axis hinge is evaluated, as shown in Figure 9(a) to (d). In

addition, one end of the hinge is fixed and the free end is subject to external forces. The geometry centre of the notch is located at  $x = l_1 + l_2/2$ . It is worth mentioning that the instant rotation centre depends on the notch profile and the external load. In order to compare the performance of hinges with different notch profiles, the unit moment condition (e.g.  $M_z = 1$  N·m, as shown in Figure 9(a)) is modelled. It is assumed that all parts except the notch profile are sufficiently rigid and the axial deformation is neglected. At this case, the straight line through the free end (point  $Q_2$ ) and perpendicular to the rigid block can be expressed as<sup>36</sup>

$$y - M_z C_{\Delta y-M_z} = (x - L) \tan(M_z C_{\theta z-M_z}). \quad (55)$$

Then, the intersection of the straight line and the horizontal axis  $O_1-x$  is the instant rotation centre of the hinge, whose  $x$ -coordinate position can be expressed as

$$l_{rc} = L - \frac{M_z C_{\Delta y-M_z}}{\tan(M_z C_{\theta z-M_z})}. \quad (56)$$

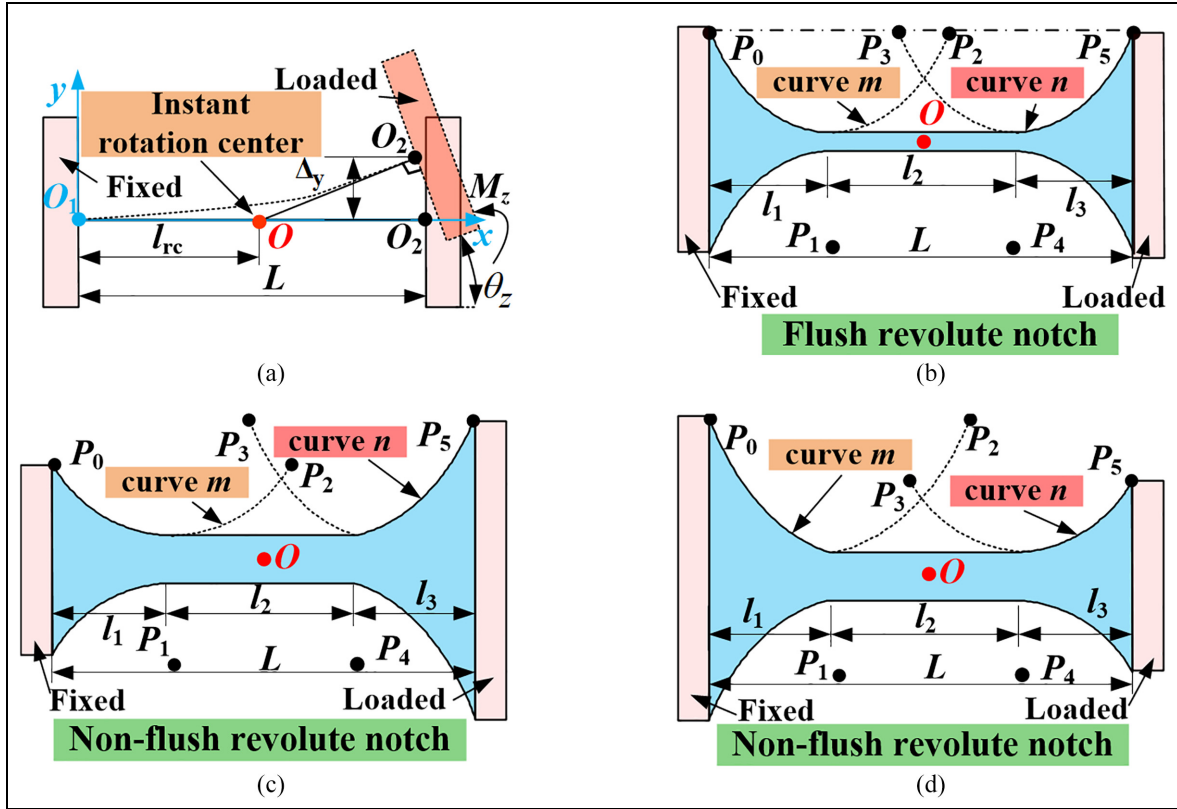


**Figure 9.** Precision of rotation: (a) rotation center, (b) flush revolute notch (c) non-flush revolute notch and (d) non-flush revolute notch.

In order to compare the precision characteristics between hybrid flexure hinges, the dimensionless ratio representing the instant relative position of the rotation centre can be expressed as

$$R_{L-rc} = \frac{l_{rc}}{L}. \quad (57)$$

In order to quantitatively evaluate the performance of flexure hinges with different notch profiles, some constraints need to be imposed. In other words,  $L$  and  $d_{min}$  are constant. Also, set  $l_1 = l_3$ . In this case, the notch profile is changed by using the weight  $w$ , as shown in Figure 10(a). Besides, based on the previous analysis, whether the notch profile is flush or not is considered, as shown in Figure 9(c) and (d).

As shown in Figure 10(b) to (d), the ideal rotation centre (the dimensionless ratio  $R_{L-rc} = 0.5$ ) is used as a reference. It should be noted that the closer the dimensionless ratio  $R_{L-rc}$  is to the reference, then the higher the rotational precision of the hinge. As shown in Figure 10(c) and (d), how the fixed and free ends of the hinge are set can make the rotational precision affected. In addition, the dimensionless ratio  $R_{L-rc}$  decreases with increasing  $w_n$  and decreases with increasing  $w_m$ . Further, the optimal choice of curves  $m$  and  $n$  should be ellipse and hyperbola, regardless of whether the components of the notch profile contain

the straight line ( $l_2 = 0$  is satisfied or not). In addition, the dimensionless ratio  $R_{L-rc}$  increases with increasing  $l_2$ . Therefore, the notch profile that does not contain the straight line ( $l_2 \neq 0$ ), regardless of whether the notch profile is flush or not. Therefore, when  $l_2 \neq 0$ , the flexure hinge has the highest rotational precision with a notch profile consisting of ellipse, a straight line and hyperbola. As shown in Figures 3 and 10, the flexure hinge has the highest rotational precision with a notch profile consisting of ellipse and hyperbola.<sup>5</sup>

### Stress equations

In order to evaluate the fatigue life of the flexure hinge, the stress should be explicitly given. As shown in Figure 1, one end of the hinge is fixed and the load is applied to the other end. The stress calculation is also different for flexure hinges with different notch profiles, which is mainly due to stress concentrations. It should be noted that the stress concentration factor of single-axis flexure hinges has been investigated.<sup>40</sup> Here, the maximum stress  $\sigma_{max}$  resulting from tension/compression and bending can be expressed as

$$\sigma_{max} = \frac{32k_b [M_y + M_z + (F_y + F_z)L]}{\pi d_{min}^3} + \frac{4k_a F_x}{\pi d_{min}^2}. \quad (58)$$

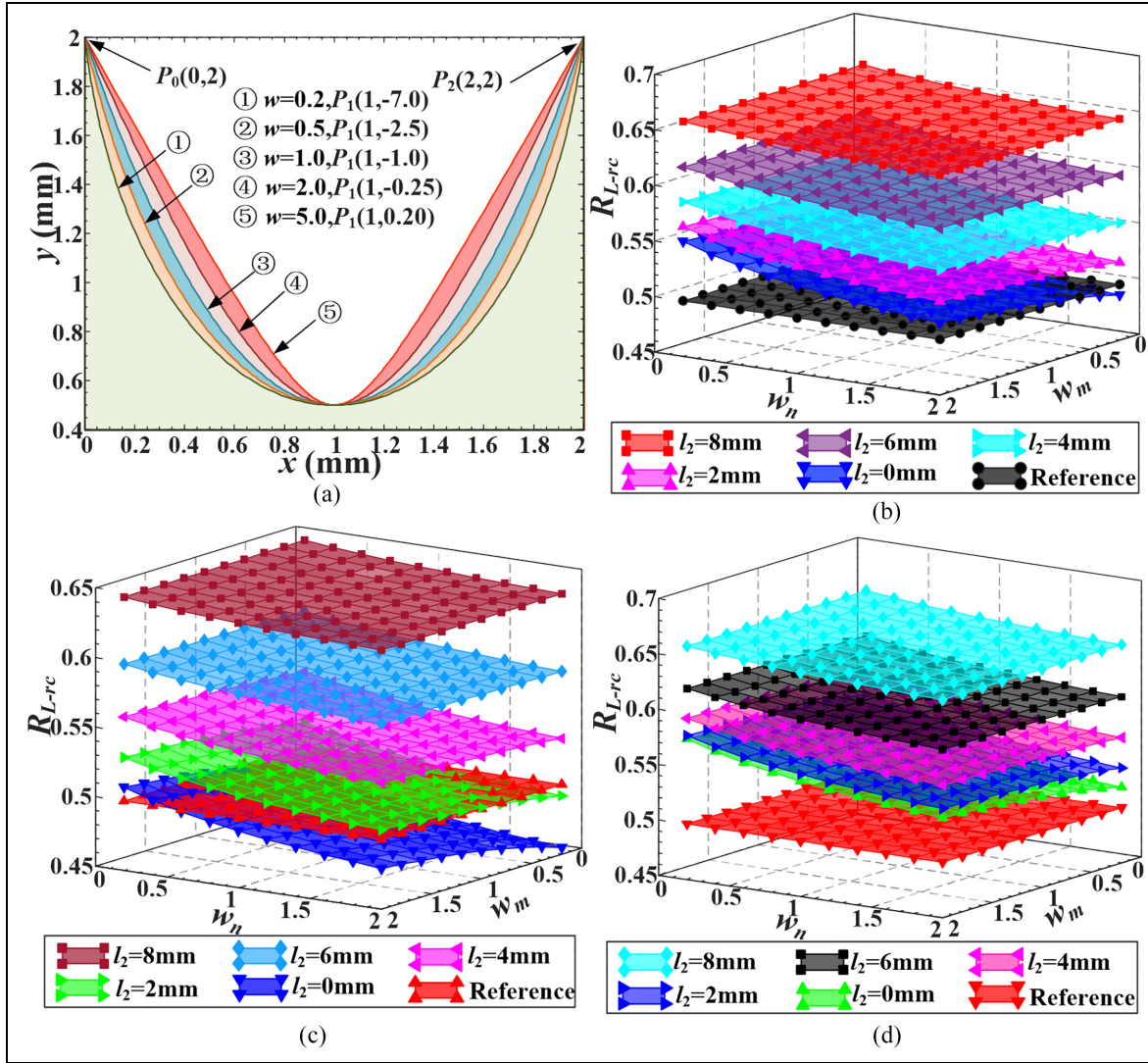


**Figure 10.** The instant relative position of the rotation centre: (a) curvature-adjustable notch profiles, (b)  $y_0 = y_2 = y_3 = y_5$ , (c)  $y_0 = y_2 < y_3 = y_5$  and (d)  $y_0 = y_2 > y_3 = y_5$ .

Furthermore, the maximum stress  $\tau_{\max}$  resulting from torsion can be expressed as

$$\tau_{\max} = \frac{16k_t M_x}{\pi d_{\min}^3}. \quad (59)$$

It is important to be noted that  $k_b$  (in bending),  $k_a$  (in tension/compression), and  $k_t$  (in torsion) are stress concentration factors.<sup>41</sup>

## Conclusion

In this paper, a curvature-adjustable multiple-axis flexure hinge is proposed based on Bézier curve. The curvature-adjustable property can be applied to the design of multiple-axis hinges with common notch profiles, which are mainly composed of circles, ellipses, hyperbolas, and parabolas. Thus, the hinge has a wider range of applications than the existing.

In addition, a simplified classification method of notch profile is proposed based on the binary quadratic implicit equation, which is convenient to determine the type and structural parameters of notch profiles. The method provides a very simple and effective reference for the design and CNC machining process of hinges. Then, the structural parameters of 12 typical flexure hinges are designed based on the previous analysis. And the correctness of all compliance equations is further verified using finite element analysis. The results show that the maximum relative error between the analytical results and the finite element analysis is 6.07%.

Finally, the compliance, the precision of rotation, and stress are investigated based structure parameters. The results show that the change in the rotation centre does not significantly affect the axial and bending compliance ( $C_{\Delta x-Fx}$ ,  $C_{\theta z-Mz}$ ,  $C_{\theta y-My}$ ,  $C_{\theta x-Mx}$ ) for multiple-axis flexure hinges with a specific single and flush Bézier curve notch profile. Then, the flexure

hinge has the highest rotational precision with a notch profile consisting of ellipse and hyperbola. The results provide a potential method for designing spatial compliant micro–nano mechanisms.

### Declaration of conflicting interests

The author(s) declared no potential conflicts of interest with respect to the research, authorship, and/or publication of this article.

### Funding

The author(s) disclosed receipt of the following financial support for the research, authorship, and/or publication of this article: This work was supported by National Natural Science Foundation of China ([No.11972343], [No.62235018]) and Jilin Scientific and Technological Development Program [No.20220204116YY].

### ORCID iD

Xuwen Wang  <https://orcid.org/0000-0002-7422-6366>

### References

- Wang X, Yu Y, Xu Z, et al. Design and assessment of a micro-nano positioning hexapod platform with flexure hinges for large aperture telescopes. *Opt Express* 2023; 31: 3908–3926.
- Wei L, Yu L, Wang J, et al. An FBG-sensing two-dimensional vibration sensor based on multi-axis flexure hinge. *IEEE Sens J* 2019; 19: 3698–3710.
- Lei Y-J, Li RJ, Chen R-X, et al. A high-precision two-dimensional micro-accelerometer for low-frequency and micro-vibrations. *Precis Eng* 2021; 67: 419–427.
- Dan W and Rui F. Design and nonlinear analysis of a 6-DOF compliant parallel manipulator with spatial beam flexure hinges. *Precis Eng* 2016; 45: 365–373.
- Ma W, Wang R, Zhou X, et al. The performance comparison of typical notched flexure hinges. *Proc IMechE, Part C: J Mechanical Engineering Science* 2020; 234: 1859–1867.
- Schotborgh WO, Kokkeler FGM, Tragter H, et al. Dimensionless design graphs for flexure elements and a comparison between three flexure elements. *Precis Eng* 2005; 29: 41–47.
- Yong YK, Lu TF and Handley DC. Review of circular flexure hinge design equations and derivation of empirical formulations. *Precis Eng* 2008; 32: 63–70.
- Chen G, Liu X and Du Y. Elliptical-arc-fillet flexure hinges: toward a generalized model for commonly used flexure hinges. *J Mech Des* 2011; 133: 133.
- Chen G, Shao X and Huang X. A new generalized model for elliptical arc flexure hinges. *Rev Sci Instrum* 2008; 79: 095103.
- Fu J, Yan C, Liu W, et al. Simplified equations of the compliant matrix for right elliptical flexure hinges. *Rev Sci Instrum* 2015; 86: 115115.
- Smith ST, Badami VG, Dale JS, et al. Elliptical flexure hinges. *Rev Sci Instrum* 1997; 68: 1474–1483.
- Chen Z, Chen G and Zhang X. Damped leaf flexure hinge. *Rev Sci Instrum* 2015; 86: 055002.
- Freire Gómez J, Booker JD and Mellor PH. 2D shape optimization of leaf-type crossed flexure pivot springs for minimum stress. *Precis Eng* 2015; 42: 6–21.
- Lobontiu N, Paine JSN, Garcia E, et al. Corner-filletted flexure hinges. *J Mech Des* 2001; 123: 346–352.
- Meng Q, Li Y and Xu J. A novel analytical model for flexure-based proportion compliant mechanisms. *Precis Eng* 2014; 38: 449–457.
- Chen G, Liu X, Gao H, et al. A generalized model for conic flexure hinges. *Rev Sci Instrum* 2009; 80: 055106.
- Lobontiu N, Paine JSN, Garcia E, et al. Design of symmetric conic-section flexure hinges based on closed-form compliance equations. *Mech Mach Theory* 2002; 37: 477–498.
- Lobontiu N, Paine JSN, O'Malley E, et al. Parabolic and hyperbolic flexure hinges: flexibility, motion precision and stress characterization based on compliance closed-form equations. *Precis Eng* 2002; 26: 183–192.
- Tian Y, Shirinzadeh B and Zhang D. Closed-form compliance equations of filleted V-shaped flexure hinges for compliant mechanism design. *Precis Eng* 2010; 34: 408–418.
- Tian Y, Shirinzadeh B, Zhang D, et al. Three flexure hinges for compliant mechanism designs based on dimensionless graph analysis. *Precis Eng* 2010; 34: 92–100.
- Tseytlin Y. Note: Rotational compliance and instantaneous center of rotation in segmented and V-shaped notch hinges. *Rev Sci Instrum* 2012; 83: 026102.
- Li Q, Pan C and Xu X. Closed-form compliance equations for power-function-shaped flexure hinge based on unit-load method. *Precis Eng* 2013; 37: 135–145.
- Chen G-M, Jia J-Y and Li Z-W. On hybrid flexure hinges. In: *Proceedings 2005 IEEE networking, sensing and control*, 19–22 March 2005, pp.700–704. New York, NY: IEEE.
- Chen G-M, Jia J-Y and Li Z-W. Right-circular corner-filletted flexure hinges. In: *IEEE International conference on automation science and engineering*, 1–2 August 2005, pp.249–253. New York, NY: IEEE.
- Wang R, Zhou X and Zhu Z. Development of a novel sort of exponent-sine-shaped flexure hinges. *Rev Sci Instrum* 2013; 84: 095008.
- Wang R, Zhou X, Zhu Z, et al. Development of a novel type of hybrid non-symmetric flexure hinges. *Rev Sci Instrum* 2015; 86: 085003.
- Kong J, Huang Z, Xian X, et al. Generalized model for conic-V-shaped flexure hinges. *Sci Prog* 2020; 103: 003685042098121.
- Wu J, Zhang Y, Cai S, et al. Modeling and analysis of conical-shaped notch flexure hinges based on NURBS. *Mech Mach Theory* 2018; 128: 560–568.
- Li L, Zhang D, Guo S, et al. Design, modeling, and analysis of hybrid flexure hinges. *Mech Mach Theory* 2019; 131: 300–316.
- Li L, Zhang D, Guo S, et al. A generic compliance modeling method for two-axis elliptical-arc-filletted flexure hinges. *Sensors* 2017; 17: 2154.
- Liang C, Wang F, Huo Z, et al. A 2-DOF monolithic compliant rotation platform driven by piezoelectric actuators. *IEEE Trans Ind Electron* 2020; 67: 6963–6974.
- Tuo W, Li X, Ji Y, et al. Mechanical design and determination of bandwidth for a two-axis inertial reference unit. *Mech Syst Signal Process* 2022; 172: 108962.

33. Li L, Zhang D, Qu H, et al. Generalized model and configuration design of multiple-axis flexure hinges. *Mech Mach Theory* 2022; 169: 104677.
34. Wang H, Wu S and Shao Z. Analytical compliance equations of generalized elliptical-arc-beam spherical flexure hinges for 3D elliptical vibration-assisted cutting mechanisms. *Materials* 2021; 14: 5928.
35. Wei H, Shirinzadeh B, Tang H, et al. Closed-form compliance equations for elliptic-revolute notch type multiple-axis flexure hinges. *Mech Mach Theory* 2021; 156: 104154.
36. Wei H, Yang J, Wu F, et al. Analytical modelling and experiments for hybrid multiaxis flexure hinges. *Precis Eng* 2022; 76: 294–304.
37. Ling M, Yuan L, Lai J, et al. Compliance and precision modeling of general notch flexure hinges using a discrete-beam transfer matrix. *Precis Eng* 2023; 82: 233–250.
38. Ling M, Yuan L and Zhang X. Bionic design of a curvature-adjustable flexure hinge inspired by red blood cells. *Precis Eng* 2023; 81: 124–134.
39. Anwar Y, Tasman H and Hariadi N. Determining implicit equation of conic section from quadratic rational Bézier curve using Gröbner basis. In: *International conference on mathematical and statistical sciences 2021 (ICMSS 2021)*, 15–16 September 2021, p.012017. IOP Publishing Inc.
40. Chen G, Wang J and Liu X. Generalized equations for estimating stress concentration factors of various notch flexure hinges. *J Mech Des* 2014; 136: 031009.
41. Pilkey WD, Pilkey DF and Bi Z. *Peterson's stress concentration factors*. New York: John Wiley & Sons, 2020.